CrystEngComm

Room Temperature Synthesis of χ-Al2O3 and Ruby (α-Cr:Al2O3)

Journal:	*CrystEngComm*
Manuscript ID	CE-ART-03-2018-000360.R2
Article Type:	Paper
Date Submitted by the Author:	17-May-2018

Complete List of Authors:	Cortes Vega , Fernando; Universidad Michoacana de San Nicolas de Hidalgo, Instituto de Investigaciones Metalúrgicas Yang, Wenli; University of Texas Dental Branch at Houston, Department of Electrical and Computer Engineering, University of Houston, Houston, TX, USA Zarate Medina, Juan; Universidad Michoacana de San Nicolas de Hidalgo, Instituto de Investigaciones Metalúrgicas Brankovic, Stanko; University of Houston College of Liberal Arts and Social Sciences, Department of Electrical and Computer Engineering Herrera Ramirez, Jose ; Centro de Investigación en Materiales Avanzados, CIMAV, Advanced Materials Robles-Hernandez, Francisco; University of Houston, Mechanical Engineering Technology

Room Temperature Synthesis of χ-Al_2O_3 and Ruby (α-Cr:Al_2O_3)

Fernando D. Cortes-Vega[1,2], Wenli Yang[3], Juan Zarate-Medina[2], Stanko R. Brankovic[3], José M. Herrera Ramírez[4], Francisco C. Robles-Hernandez[1,3,5,*]

[1]*Department of Mechanical Engineering Technology, University of Houston, Houston, TX, USA*

[2]*Instituto de Investigación en Metalurgia y Materiales, Universidad Michoacana de San Nicolás de Hidalgo, Ciudad Universitaria, Michoacán, México*

[3] *Department of Electrical and Computer Engineering, University of Houston, Houston, TX, USA*

[4] *Centro de Investigación en Materiales Avanzados, CIMAV, Chihuahua Mexico*

[5] *Department of Materials Science and Engineering, University of Houston, Houston, TX, USA*

[*] To whom the correspondence should be addressed to: fcrobles@uh.edu

Abstract

In this work we present a unique crystal growth synthesis of χ-Al_2O_3 at room temperature accompanied with α-$Cr{:}Al_2O_3$. Raman spectroscopy and additions of Cr_2O_3 are key to identify α-$Cr{:}Al_2O_3$ in trace amounts by the room temperature synthesis of ruby (α-$Cr{:}Al_2O_3$). The presence of this phase is further confirmed with HRTEM. The raw materials are pseudoboehmite and Cr_2O_3 that are treated mechano-chemically for the successful synthesis of ruby and χ-Al_2O_3. A thermal analysis approach is provided to explain the significant temperature reduction for the complete transformation to α-$Cr{:}Al_2O_3$ during annealing. The α-$Cr{:}Al_2O_3$ synthesized at room temperature act as seed or hetero sites for nucleation and are responsible of a temperature drop of approximately 200 °C (to 867 °C). This material is ideal for optical, photonics, defense, energy storage and harvesting among other strategic applications.

Keywords: Al_2O_3, ceramics, synthesis, mechanical milling, residual stresses.

Introduction

Alumina is one of the most abundant and widely used ceramics, having wide range of applications from cooking ware to catalysis, electronics, medical, optics, aerospace, defense among others [1-4]. The outstanding hardness and stability of alumina(s) (Al_2O_3) allows their use under extreme environments such as high temperatures, highly corrosive environments, compressive stresses, etc. These characteristics make alumina desirable for many uses where the word nano is a common prefix [5-8]. Naturally occurring alumina is the second hardest material, just after diamond. The α-Al_2O_3 and Cr_2O_3 form a complete solution in solid and liquid states [1, 9, 10]. Their solid solution is commonly known as ruby and forms by the substitution of Al^{3+} for Cr^{3+} in octahedral sites [10, 11]. The formation of the solid solution involves a small expansion of the α-Al_2O_3 lattice, owing to the comparatively larger ionic radius of Cr^{3+} [12].

Ruby is well known for its resonant luminescent bands (R_1 and R_2) that are easily detectable with Raman spectroscopy. These bands are known for their sensitivity to shift with temperature and pressure [13-17]. This characteristic makes ruby highly desirable material, not only as a gemstone, but also as a sensor with applications under extreme conditions (e.g. pressure and temperature). Conventionally, ruby is synthesized out of α-Al_2O_3 (corundum) with Cr^{3+} additions at temperatures of at least 1200 °C. Here we present a unique methodology to synthesize significant amounts of this phase at room temperature. However, for the complete transformation one need to heat treat the material. Yet, the transformation occurs at approximately 193 °C below the typical phase transition temperature. The process presented herein is able to synthesize χ-Al_2O_3 at room temperature using pseudoboehmite as precursor. During the milling process a full dehydroxylation occurs at room temperature. This process is usually observed at temperatures between 300 and 500 °C [18-26]. Hitherto, for the first time we demonstrated that this transformation can be accomplished at room temperature, purely by milling, in the absence of other Al_2O_3 phases such as $\theta, \gamma, \kappa, \delta$.

We report the room temperature phase transformations of pseudoboehmite to χ-Al_2O_3 and ruby (α-Cr:Al_2O_3) based purely by milling in SPEX. The complete transformation to χ-Al_2O_3 is evident in samples milled for approximately 30 h. In the milled samples one can observe the presence of α-Cr:Al_2O_3. This phase is identifiable in samples milled for as little as 5 h. However, the presence of α-Cr:Al_2O_3 is in small fractions, perhaps traces that are undetectable by XRD. Here is a major novelty of our work, as we added traces of Cr_2O_3 to purposely synthesize ruby that can be detected by Raman spectroscopy. The detection of parts per million amounts of ruby is possible with Raman. This work demonstrates four major findings: the room temperature synthesis of i) χ-Al_2O_3 and ii) α-Cr:Al_2O_3 with SPEX, iii) the changes in phase transformation energy requirements and iv) a 193 °C drop in phase transformation temperature from χ-Al_2O_3 to α-Al_2O_3.

Results and Discussions

Figure 1 shows the XRD spectra for the raw pseudoboehmite and the milled samples. Room temperature milling is capable of fully transforming pseudoboehmite into χ-Al_2O_3 for times as short as 30 h. The χ-Al_2O_3 is a unique phase not well investigated and it is not typically found in non-heat treated samples. The pseudoboehmite shows the following 7 diffracting planes: (020), (120), (031), (200), (151), (002) and (251) that is in agreement with the XRD reference pattern (21-1307 JCPDS). Yet, the (020) is slightly shifted toward lower angles in comparison to the crystalline boehmite. This shift is attributed to the presence of interlayers of water [27-29]. Therefore, due to the excess of water in the lattice we conclude that we do not have boehmite; instead, we have pseudoboehmite.

Pseudoboehmite has an orthorhombic crystalline structure with the oxygen in anionic arrangements and the aluminum cations in the octahedral sites. The relatively low concentration of Cr_2O_3 is untraceable by XRD. Figure 1 shows evidences of the effects of mechanical milling time in the broadening of the reflections that is translated into a reduction in grain size. This effect is observed even at low milling times (5 h). What is unique is the transformation to χ-Al_2O_3 at room temperature. In the literature, the χ-Al_2O_3 has been reported at temperatures between 300 and 500 °C [30-32].

The identification of χ-Al_2O_3 is carried by comparing the experimental XRD with that reported in 13-0373 JCPDS. In the sample milled for 30 h the pseudoboehmite is no longer discernible; instead, the χ-Al_2O_3 phase is the only observable phase. This is the first report, as we are concern, of this transformation at room temperature.

The typical pseudoboehmite reflections corresponding to the planes (151) and (251) are no longer present after 10 h of milling that results by the transformation to χ-Al_2O_3. However, the reflections become predominant after 30 h of milling. This phase transformation path is unique to mechanical milling [33] and the obtained χ-Al_2O_3 does not have traceable amounts of other phases such as $\theta, \gamma, \kappa,\ and\ \delta$. Those phases are typically found when the transformation is done using other precursors and heat treatments. In parallel experiments, when we heat treat our samples the transformation follows the following path: pseudoboehmite → δ-Al_2O_3 → α-Al_2O_3. In the milled samples the transformation is as follows: pseudoboehmite → χ-Al_2O_3 → α-Al_2O_3. It means no evidence of γ-Al_2O_3 is observed.

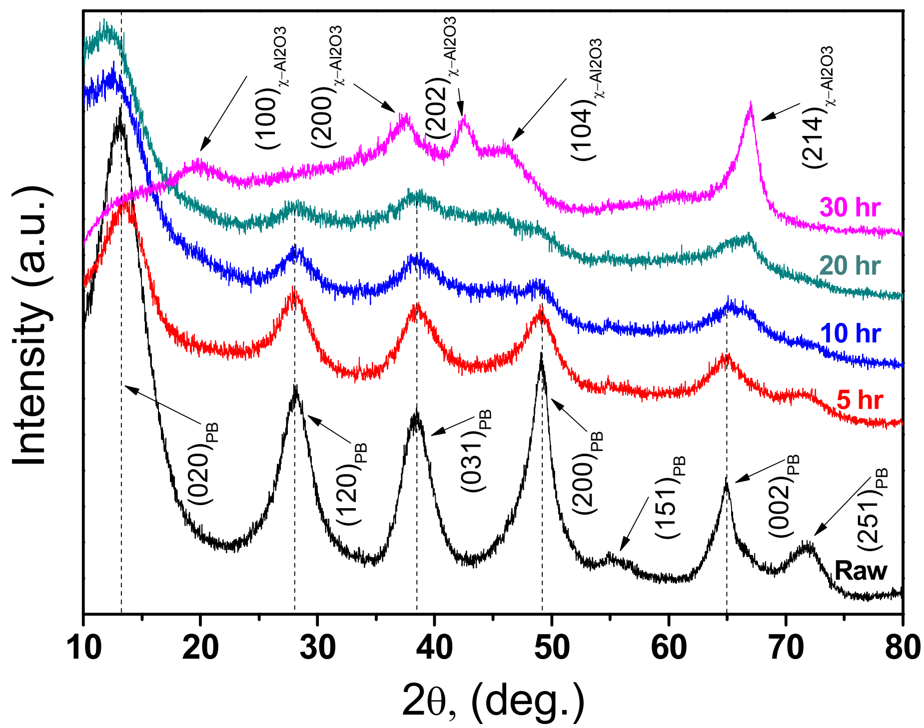

Figure 1. Diffraction patterns of the raw and milled samples. PB and χ-Al_2O_3 stand for pseudoboehmite and chi-alumina respectively.

Figure 2 shows the Raman spectra of the analyzed samples in the range of 300 cm^{-1} to 800 cm^{-1}. The raw sample showed three active modes (A_g+B_{1g}+B_{3g}) assigned to the most prominent bands of pseudoboehmite detected at ~364 cm^{-1}, 488 cm^{-1} and 683 cm^1 [34]. Only one vibrational mode (A_{1g}) for Cr_2O_3 is discernible at ~563 cm^{-1} [8], the relative intensity is attributed to the relatively low concentration.

The mechanical milling affected the structure of pseudoboehmite, generating their vibrational modes to shift to lower frequencies. This shift is evident in milling times as short as five hours. At higher milling times the intensity of the vibrational modes of pseudoboehmite decrease, which suggest a reduction on the crystal quality or a grain refining effect. From figure 2 is observed that the A_{1g} band of Cr_2O_3 changes with the milling time. This band is detected in the raw sample pseudoboehmite+Cr_2O_3 and in milled samples for up to 10 h. After 20 h of milling the band of Cr_2O_3 is no longer traceable. Here we associate the absence of the A_{1g} mode to the rupture of the Cr_2O_3 that generates ions Cr^{+3} and substitute the Al^{+3} in the host lattice. In order to identify the effects of Cr_2O_3, the Raman range needs to be changed to luminescent range for ruby that is between 4300 and 4500 cm^{-1} (Figure 3a).

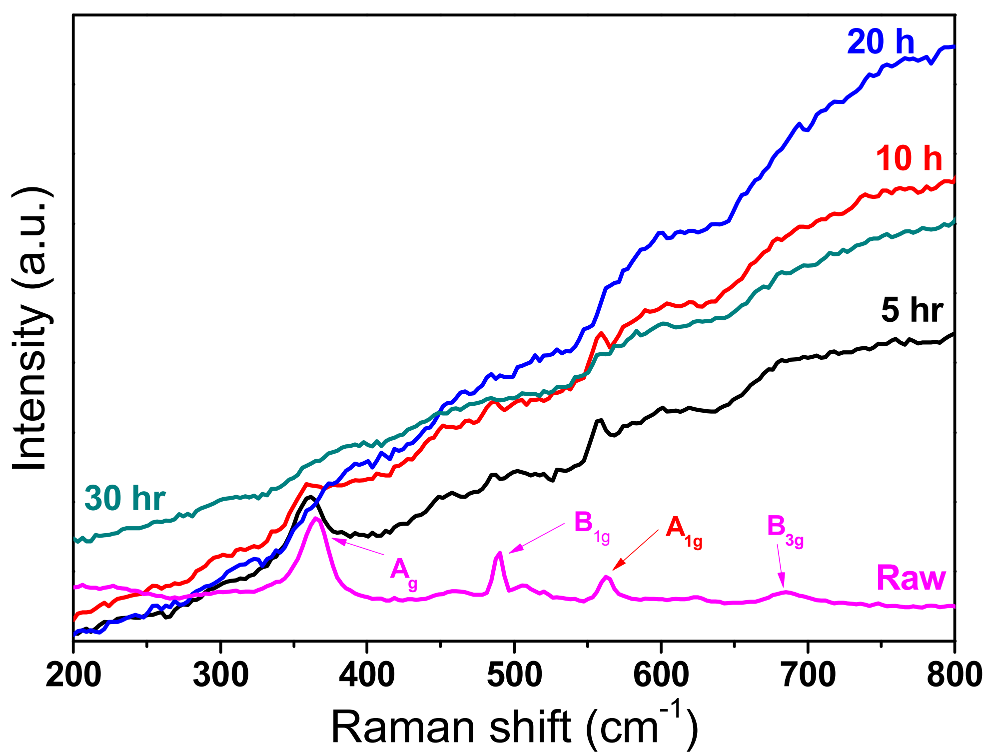

Figure 2. Raman spectra of Raw and milled samples with an excitation line of 532 nm. All the identified bands are associated with pseudoboehmite; except, for A_{1g} that is typical of Cr_2O_3.

Figure 3a shows the Raman analysis in the range of 4300 cm^{-1} to 4500 cm^{-1} that is the location where we expect to observe the luminescent bands R_1 and R_2. The presence of those bands demonstrate that the Cr_2O_3 sponsored the synthesis of α-$Cr:Al_2O_3$ (in this case ruby) at room temperature. The R_1 and R_2 bands show relatively high intensity, making possible the detection of ruby phase in few parts per millions, which is rather challenging by other methods. Therefore, Raman spectroscopy is a highly desirable method to characterize this phase. Detecting the bands R_1 and R_2 is essential because they are characteristics of the substitutional Cr^{3+} ions that are unique to the substitution in the octahedral sites of α-Al_2O_3. Both, the phase transformation and its successful identification in room temperature approaches make this research unique.

The luminescence is an optical emission that involves the electron transitions between the states $^4A_2$ (ground state), $^4T_2$ (short lived state) and ^2E (metastable state) as explained in Figure 3c. Figure 3c sketches the luminescence mechanism observed in the presence of an excitation line, e.g. 532 nm, and the emitted R_1 and R_2 bands. This may be explained in terms of the crystal field theory, which dictates that the crystal field stabilization energy (CFSE) presents its maximum in the case of octahedral sites for d3 (Cr^{+3}) [35]. Both bands, R_1 and R_2, are clearly discernible in all milled samples and they are not present in the raw sample. The intensity of both bands increases with milling time and is proportional with the amount of ruby in the sample. To identify this phase we need only 5 h of milling. The intensity of the peaks and their easy detection increases with time as well. This demonstrates the dynamic transformation from χ-Al_2O_3 into α-$Cr:Al_2O_3$.

The discernibility of the bands is related to the higher crystallinity of the solid solution. This, in parallel, translates in the extinction of the A_{1g} mode of Cr_2O_3 (Figure 2). On the other hand, the χ-Al_2O_3 is gaining crystal quality as shown in Figure 1. Though, pure α-Al_2O_3 is untraceable unless it is doped with Cr^{3+}. Patra et al. [36] showed that the crystalline ruby affects strongly the shape of the luminescent lines R_1 and R_2. They also propose that the substitutional Cr^{+3} ions in the octahedral sites of the δ-Al_2O_3 and θ-Al_2O_3 phases do not generate the R_1 and R_2 resonant bands. Instead, they exhibit only a broad band [36]. This again demonstrates that we are producing ruby at room temperature by a new green and purely mechanical method.

In figure 3b are plotted the intensities of the R_1 and R_2 lines as a function of the milling time. The observed behavior shows that the formation of the solid solution increases linearly until 20 hr of milling. The intensity of the R_1 and R_2 bands increase abruptly (exponential) in the sample milled for 30 hr. This increase is approximately 13 folds when comparing the samples milled 20 h. Besides the fact that after 30 h the pseudoboehmite is rather untraceable by XRD and confirmed by Raman, we conclude that all the pseudoboehmite has transformed into χ-Al_2O_3 and α-$Cr:Al_2O_3$.

In Figure 4 we present a micrograph under high resolution transmission electron microscopy (HRTEM) for the samples milled for 30 h. The image shows a by-crystal framework clearly identifying both phases in the investigated sample: χ-Al_2O_3 and α-$Cr:Al_2O_3$. Furthermore, in HRTEM we did not observe pseudoboehmite that is in agreement with the XRD and Raman results. This result further confirms the successful synthesis of α-Cr:Al_2O_3 by room temperature milling. The HRTEM micrographs also agree that the sample is nanostructured. The presence of ruby under HRTEM is a clear demonstration of the potential of milling to synthesize ruby at room temperature.

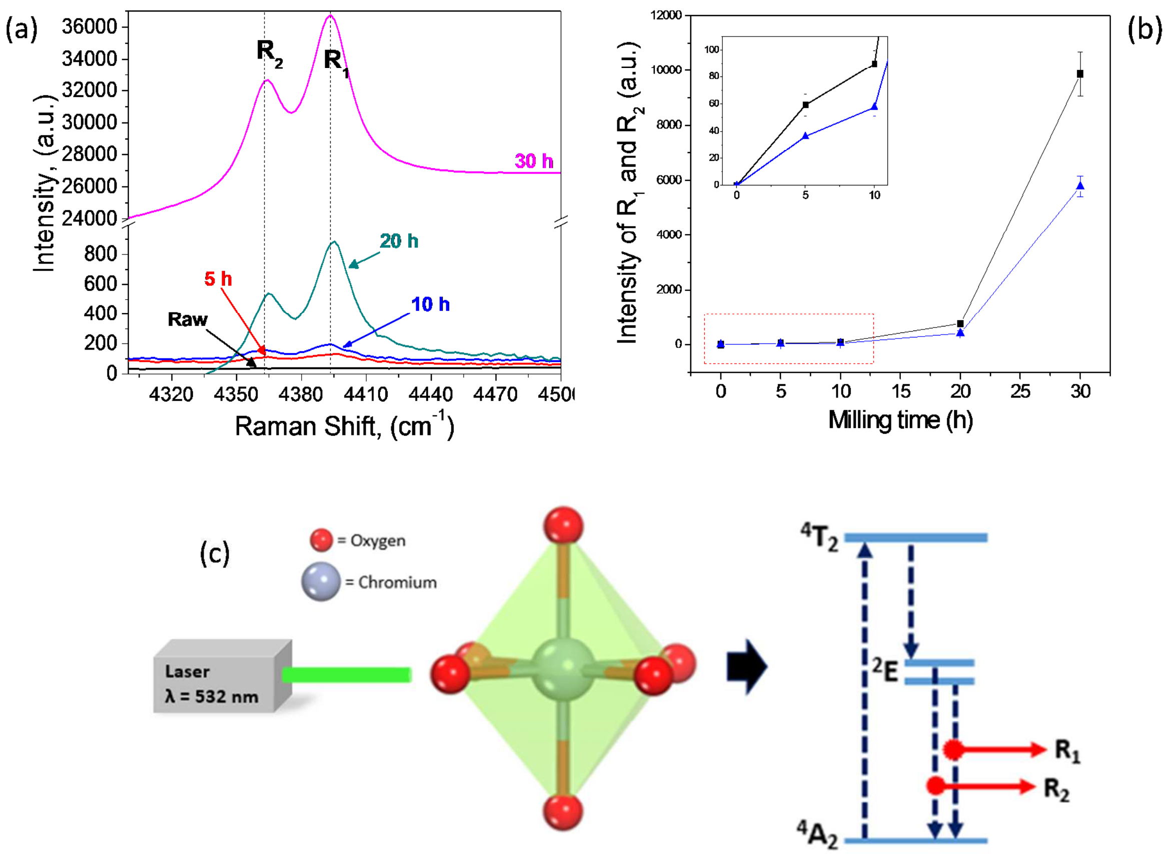

Figure 3. (a) Raman spectra of Raw and milled samples for up to 30 h and (b) change of intensity (R_1 and R_2) as a function of milling time. Note the difference in intensity for the spectra obtained in samples milled for up to 20 h to that milled for 30 h. c) Mechanism of luminescence of ruby excited with a green laser of 532 nm.

The HRTEM image shows two main particles that are analyzed by means of FFT to produce their respective diffraction patters. The FFT image is then converted into the

IFFT to generate filtered and hence clearer images from the areas labeled (i) and (ii). The analysis of area (i) matches with the characteristics of α-Al_2O_3. On the other hand the area (ii) corresponds to χ-Al_2O_3. The inset in the IFFT image for (i) has a clear match with the simulated structure that is presented over the HRTEM image. Unfortunately, we cannot generate the same image for χ-Al_2O_3 because this phase is not well investigated and the space group of this phase has not been reported. The space group is fundamental to identify the actual crystalline structure and it is also mandatory in order to simulate the respective structures. It is known that χ-Al_2O_3 matches with the expected phase according to the JCPDS chart for χ-Al_2O_3. The results agree with XRD and Raman allowing to confirm the room temperature synthesis of χ-Al_2O_3 and α-Cr:Al_2O_3.

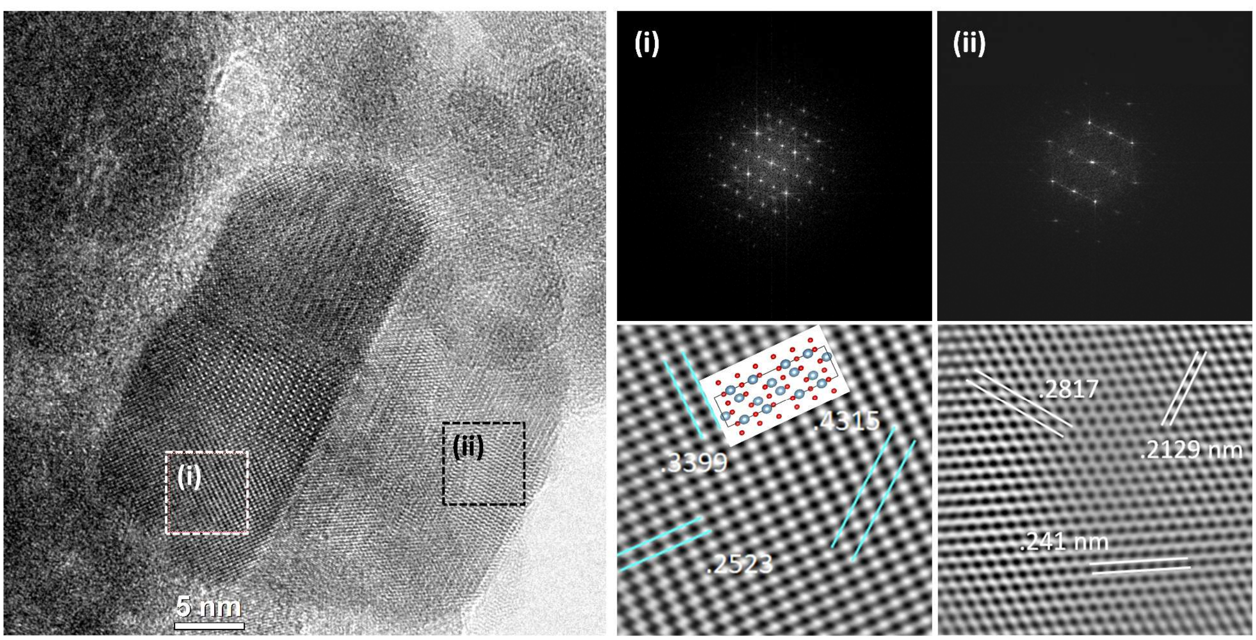

Figure 4. HRTEM images and interplanar measurements for α-Cr:Al_2O_3 (i) and χ-Al_2O_3 (ii) with respective FFT images for each location showing the presence of each phase.

Figure 5 shows the thermal analyses results where it is monitored the complete transformation to α-Cr:Al_2O_3 from the raw and the sample milled for 30 h. The 30 h sample is used for this analysis to enhance the differences in phase transformations among when compared to the raw sample. A major finding herein is the different phases transforming during the annealing process for the raw and milled samples. The raw sample shows the water evaporation and the dehydroxylation along with the transformation to δ-Al_2O_3, and then, α-Cr:Al_2O_3. The milled sample shows a combined endotherm for the water loss and dehydroxyliation, which is followed by χ-Al_2O_3, κ-Al_2O_3 and finally α-Cr:Al_2O_3.

The heat flow profile of the raw sample have two endothermic reactions, one for water and the second attributed to dehydroxylation. In the milled sample we observe only one endothermic process that is associated to the combined process of dehydration and dehydroxylation. This represents a reduction in the energy requirements of 58% for the milled sample to transform into χ-Al_2O_3. At higher temperatures the raw and samples milled for 30 h have the presence of the following intermediate phases δ-Al_2O_3 and κ-Al_2O_3. This phase identification is made based on the transformations reported in [37],[38]. In both cases as the temperature increases the intermediate phases transform into α-Cr:Al_2O_3.

For the milled sample the transformation to α-Cr:Al_2O_3 initiates at approximately 867 ºC and concludes at 1163 ºC. In the case of the raw sample the same reaction initiates at 1060 ºC and ends at 1190 ºC. This represents a reduction in transformation temperature of approximately 193 ºC that is attributed to presence of α-Cr:Al_2O_3 “seeds” that are synthesized at room temperature by milling. The α-Cr:Al_2O_3 seeds are nanometric and act serve as hetero-nuclei for the high temperature α-Cr:Al_2O_3.

The energy requirements to transform κ- and δ-Al_2O_3 are exothermic, but in both cases the energy released is almost negligible. On the other hand, the transformation to α-Cr:Al_2O_3 has a significantly larger exothermic reaction (Figure 5). In a comparative analysis the increase in the internal energy released during the transformation to α-Cr:Al_2O_3 is 285 % larger in the milled sample. Therefore, this is a clear evidence that milling is an α-Cr:Al_2O_3 promoter, allowing a less demanding phase transformation process. The energies are estimated as the areas under the curves between the heat curve and the base line identified in Figure 5.

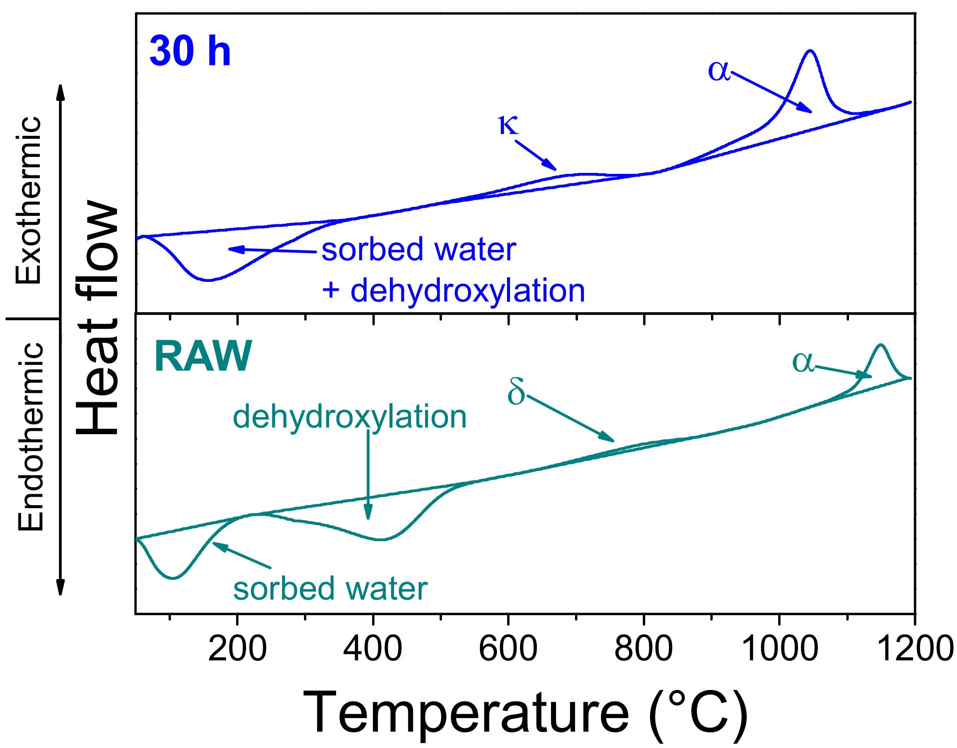

Figure 5. DSC analysis of raw and 30 h milled pseudoboehmite.

Figure 6 shows the Raman spectra for the raw sample (pseudoboehmite) and the α-Cr:Al_2O_3 powder obtained after heat treatment. The resulting vibrational modes confirm the full transformation to α-Cr:Al_2O_3 that agrees with the XRD results. All the active vibrational modes for both: pseudoboehmite and α-Cr:Al_2O_3 were successfully identified in the respective samples. Again, in the milled sample there is only a partial transformation to α-Cr:Al_2O_3 and it can only be detected by Raman spectroscopy through the Cr_2O_3 additions that are used to synthesize ruby. The presence of α-Cr:Al_2O_3 seeds are responsible for synthesis of highly crystalline alumina even at temperatures of 193 °C below the equilibrium temperature of this phase. This temperature drop is a quantum leap for optoelectronic applications as this opens a wide variety of new substrates that can be coated with sapphire or ruby. Potential applications of this material include electronic, optics, aerospace, superconductivity, and biological use. As an example of potential applications here we cite our previous work [39]. Based on the Raman spectra in Figure 6 one can say that there is no evidence of any other phase except for α-Cr:Al_2O_3. Therefore, here we no longer need to analyze the ruby in the sample; instead, we characterize α-Cr:Al_2O_3 directly. Furthermore, our results were satisfactorily checked against the Bilbao Crystallographic Server [34].

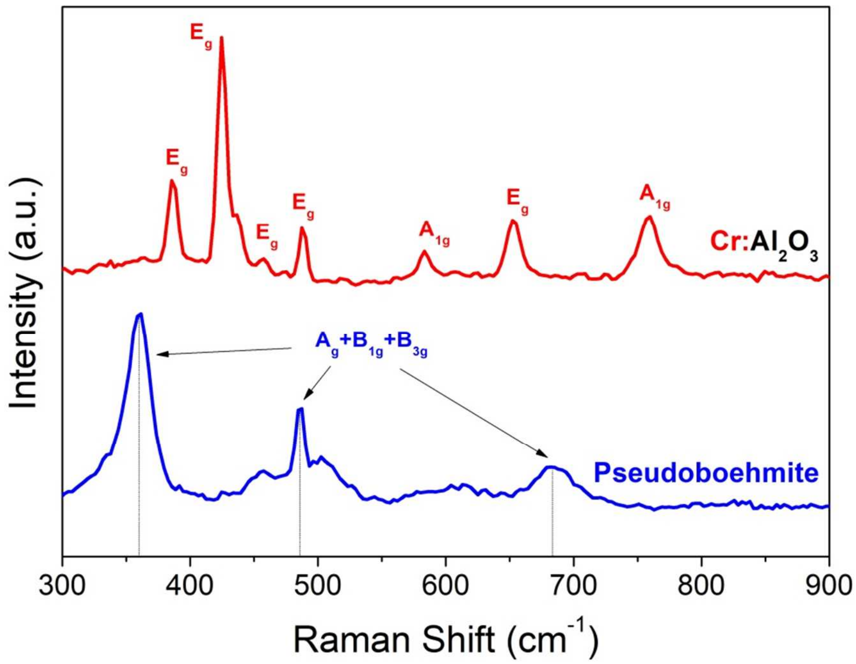

Figure 6. Raman spectrum of pseudoboehmite and α-Cr:Al_2O_3 acquired with a laser source of 532 nm.

Figure 7 shows an analysis of the shift on the luminescent lines R_2 and R_1 (compare with Fig. 3), which is associated to compressive residual stress. The residual stress build up is important factor that affects the performance of structural materials such as protective oxide barriers, thermal coatings and bulk materials. In the literature we can find several studies about the estimation of the residual stresses for different systems, not only for barriers and coatings but also for bulk materials [40, 41]. However, here we use this parameter to assess the level of residual stresses as a measure of internal energy increase. Here we present the results for the samples milled for 20 and 30 h and we compare the results to a reference sample. The reference sample was produced by annealing pure pseudoboehmite+0.2Cr_2O_3 at 1300 °C for 2 h. The conditions were set for the lowest temperature and shortest time capable of producing samples where the R_1 and R_2 bands are no longer shifting (zeroresidual stress). At the same time, this prevents excessive grain growth. This annealing is also sufficient to fully develop the solid solution (α-Cr:Al_2O_3) between α-Al_2O_3 and Cr_2O_3.

The relative change in residual stresses is used as an indirect measure of the changes in internal energy in the sample. The residual stresses attributed to the substitution of Cr^{3+} for Al^{3+} in octahedral sites contribute to the compressive state of the sample. However, this contribution is rather limited because the sample composition in both cases is similar and it is only 0.2 wt%. Therefore, the main component here is the residual stresses due to milling. In the reference sample the R_2 and R_1 bands were identified at 4367.3 cm^{-1} and 4397.0 cm^{-1}, respectively.

The longer the milling time the better define are the resonant bands due to an increase in the ruby phase. This in turn improves the resolution and accuracy of the Raman analysis. For the R_1 band (higher intensity) [42] the red shift (ΔR_1) for the sample milled for 20 h is = 2.8 cm^{-1} and for 30 h is = 4.2 cm^{-1}. Using equation 3 we calculated the respective compressive stresses

$$\Delta\nu = -7.59P \qquad (3)$$

where $\Delta\nu$ is the change of frequency in cm^{-1}, P is the pressure in GPa and -7.59 is the piezo-spectroscopic constant. The calculated values are -0.37 GPa and -0.55 GPa for the samples milled for 20 and 30 h respectively. The increase in residual stress is in agreement with the increase in internal energy as presented in the thermal analysis section. Therefore, this is a sort of measure of off-equilibrium conditions that contributed to the drop in transformation temperature to α-Cr:Al_2O_3 as well as the energy requirements for the full transformation to α-Cr:Al_2O_3. In conclusion, the increase in internal energy promotes the transformation at lower temperatures and a higher exothermic release for the phase transforming.

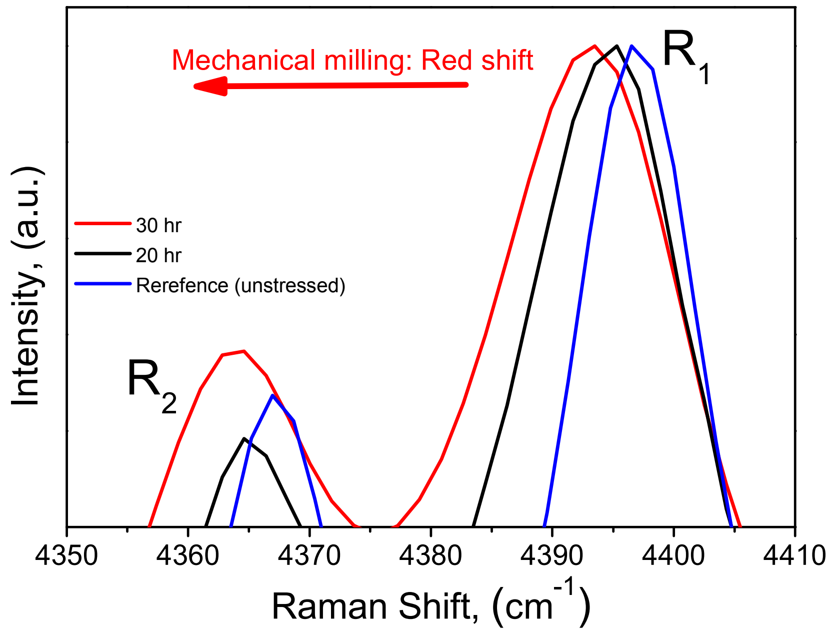

Figure 7. Raman spectra of the samples milled for 20 h and 30 h against the unstressed sample (reference).

Conclusion

In the present work is demonstrated the successful synthesis of the χ-Al_2O_3 and α-Cr:Al_2O_3 at room temperature. This is possible by means of mechanical milling of pseudoboehmite. The additions of Cr_2O_3 are the key to successfully identify the synthesized ruby by means of Raman spectroscopy. Mechanical milling supplies sufficient energy to promote partial dehydration and dehydroxylation to synthesize χ-Al_2O_3 along with the substitution of Cr^{3+} in octahedral sites, typical of Al^{3+}. Here we reported that pseudoboehmite starts to transform to χ-Al_2O_3 at times as short as 20 h of milling. However, α-Cr:Al_2O_3 or ruby transformation is observed in milling times as low as 5 h that it is traceable with Raman. Due to the limited amounts of ruby, this phase is untraceable by any other method; except fort HRTEM. Thermal analysis suggests a new synthesis route to produce ruby after heat treatment as well as a reduction in the transformation temperature of α-Cr:Al_2O_3 of approximately 193 ºC after 30 h of milling. This temperature drop is attributed to the α-Cr:Al_2O_3 hetero-nuclei that are synthesized during milling as well as an increase in internal energy.

Materials and Methods

Synthesis of Pseudoboehmite

The pseudoboehmite was synthesized from 0.2 M water based aluminum sulfate ($Al_2(SO_4)_3.xH_2O$, purity≥98% from Sigma Aldrich) solution. The solution was heated to 60 ^oC with vigorous stirring under additions of ammonia (NH_3) gas. The solution is kept at a constant pH (pH = 9-10) through the entire precipitation process. Equations 1 and 2 represent the precipitation process. At the end of the reaction, the products obtained are filtered and washed with distilled water for a number of times. The washing process is ended when the washing solution has a constant pH of 7. The resulting product is dried at 100 ^oC for 24 hr. The larger particles are then pulverized in a mortar to obtain a white and loose powder. The product is our raw material known as pseudoboehmite.

$$NH_3 + H_2O \rightarrow NH_4^+ + OH^- \qquad (1)$$

$$2Al^{3+} + 3SO_4^{2-} + 6NH_4^+ + 6OH^- \rightarrow 2AlO(OH) + 2H_2O + 3(NH_4)_2SO_4 \qquad (2)$$

Mechanical Milling

Pseudoboehmite powders were mixed with chromium oxide (Cr_2O_3, purity≥98% from Sigma Aldrich). The weight ratios among pseudoboehmite and Cr_2O_3 were 99.8:0.2% wt. respectively. Batches of 10 grams were milled into a stainless steel Spex media for up to 30 h.

Thermal analysis

The thermal analysis was performed in a SETARAM Differential Scanning Calorimeter Analyzer (DSC) equipment. The raw and 30 h milled powders were analyzed at a heating rate of 15 ºC/min up to a maximum temperature of 1200 ºC in argon atmosphere.

Structural Characterization

Characterization was carried out by means of XRD (X-ray diffraction) in a Siemens D5000 diffractometer with a Bragg-Brentano geometry and Cu-Kα radiation (λ = 1.5418 Å). The Raman spectroscopy was conducted on a confocal micro-Raman microscope Xplora^{TM}, Horiba JY. A 532 nm diode laser was used for excitation. High resolution transmission electron microscopy (HRTEM) was performed using a transmission electron microscope JEM-2200FS JEOL operated at 200 kV. The image analysis for the HRTEM micrographs is conducted using Digital Micrograph that is capable of reproducing the Fast Fourier Transformations (FFT) and their Inverse (IFFT) images for a more in depth analysis.

Acknowledgements

FCRH wishes to thank CONACyT-Mexico for the outstanding support for the fellowship and all the support for Fernando Cortes Vega to pursue PhD studies and a research Experience at the University of Houston. SRB acknowledges financial support from the National Science Foundation under the contract, CHE 1605331 and the University of Houston GEAR 2013 program.

References

[1] M. Trueba, S.P. Trasatti, Eur J Inorg Chem, (2005) 3393-3403.
[2] D.L. Trimm, A. Stanislaus, Appl Catal, 21 (1986) 215-238.
[3] H. Masuda, H. Asoh, M. Watanabe, K. Nishio, M. Nakao, T. Tamamura, Adv Mater, 13 (2001) 189-192.
[4] A. Kurella, N.B. Dahotre, J Biomater Appl, 20 (2005) 5-50.
[5] S. Chang, R.H. Doremus, L.S. Schadler, R.W. Siegel, Int J Appl Ceram Tec, 1 (2004) 172-179.
[6] S. Sōmiya, M. Kaneno, in, Academic Press, Amsterdam, 2013, pp. pages cm.
[7] S. Somiya, in, Elsevier

Ebsco Publishing [Distributor], New York

Ipswich, 2003.
[8] N.P. Bansal, American Ceramic Society., in: Ceramic transactions ; v. 220, John Wiley ;

American Ceramic Society, Hoboken, N.J.

[Westerville, Ohio], 2010, pp. ix, 312 p.
[9] A.Z.A. Azhar, L.C. Choong, H. Mohamed, M.M. Ratnam, Z.A. Ahmad, J Alloy Compd, 513 (2012) 91-96.
[10] A. Pillonnet, C. Garapon, C. Champeaux, C. Bovier, H. Jaffrezic, J. Mugnier, Journal of Luminescence, 87–89 (2000) 1087-1089.
[11] T.H. Maiman, Nature, 187 (1960) 493-494.
[12] J.W. Huang, H.W. Moos, Phys Rev, 173 (1968) 440-&.
[13] K. Syassen, High Pressure Research, 28 (2008) 75-126.
[14] B.R. Jovanic, Chemical Physics Letters, 190 (1992) 440-442.
[15] H.K. Mao, J. Xu, P.M. Bell, J Geophys Res-Solid, 91 (1986) 4673-4676.
[16] D.P. Ma, X.T. Zheng, Y.S. Xu, Z.G. Zhang, Phys Lett A, 115 (1986) 245-248.
[17] I. Fujishiro, Y. Nakamura, T. Kawase, B. Okai, Jsme Int J Iii-Vib C, 31 (1988) 136-141.
[18] Z.R. Zhang, T.J. Pinnavaia, Angew Chem Int Edit, 47 (2008) 7501-7504.
[19] S. Zhang, K.A. Khor, L. Lu, J Mater Process Tech, 48 (1995) 779-784.
[20] H.A. Calderon, I. Estrada-Guel, F. Alvarez-Ramírez, V.G. Hadjiev, F.C. Robles Hernandez, Carbon, 102 (2016) 288-296.
[21] F. Robles-Hernández, H. Calderón, in: ICCE-16 Conference, Kungming, China, 2008.
[22] Santana I.I., Robles Hernandez F.C., Garibay Febles V., C. H.A., Solid State Phenomena, 172-174 (2011) 727-732.
[23] J.S. Benjamin, Powder Metall Int, 12 (1980) 43-43.
[24] J.S. Benjamin, Mater Sci Forum, 88 (1992) 1-17.
[25] P.S. Gilman, J.S. Benjamin, Annu. Rev. Mater. Sci., 13 (1983) 279-300.

[26] C. Suryanarayana, Prog Mater Sci, 46 (2001) 1-184.
[27] W.N. Martens, R.L. Frost, J. Bartlett, J.T. Kloprogge, Journal of Materials Chemistry, 11 (2001) 1681-1686.
[28] B.R. Baker, R.M. Pearson, Journal of Catalysis, 33 (1974) 265-278.
[29] R. Tettenhorst, D.A. Hofmann, Clays and Clay Minerals, 28 (1980) 373-380.
[30] Y. Geng, T. Ablekim, P. Mukherjee, M. Weber, K. Lynn, J.E. Shield, Journal of Non-Crystalline Solids, 404 (2014) 140-144.
[31] A.K. Giri, Adv Mater, 9 (1997) 163-166.
[32] F.Q. Guo, K. Lu, Metallurgical and Materials Transactions A, 28 (1997) 1123-1131.
[33] T. Kozawa, M. Naito, Advanced Powder Technology, 27 (2016) 935-939.
[34] E. Kroumova, M.I. Aroyo, J.M. Perez-Mato, A. Kirov, C. Capillas, S. Ivantchev, H. Wondratschek, Phase Transit, 76 (2003) 155-170.
[35] A. Rastorguev, M. Baronskiy, A. Zhuzhgov, A. Kostyukov, O. Krivoruchko, V. Snytnikov, RSC Adv., 5 (2015) 5686-5694.
[36] A. Patra, R.E. Tallman, B.A. Weinstein, Optical Materials, 27 (2005) 1396-1401.
[37] P.S. Santos, H.S. Santos, S.P. Toledo, Materials Research, 3 (2000) 104-114.
[38] G.W. Brindley, The American Mineralogist 46 (1961) 14.
[39] F.D.C. Vega, P.G.M. Torres, J.P. Molina, N.M.G. Ortiz, V.G. Hadjiev, J.Z. Medinaa, F.C.R. Hernandez, J Mater Chem C, 5 (2017) 4959-4966.
[40] J.K. Odusote, L.A. Cornish, L.H. Chown, R.M. Erasmus, Corrosion Science, 70 (2013) 276-284.
[41] L.Y. Yang, L. Zheng, H.B. Guo, Corros Sci, 112 (2016) 542-551.
[42] G.K. Banini, M.M. Chaudhri, T. Smith, I.P. Hayward, Journal of Physics D: Applied Physics, 34 (2001) L122.